Available online at www.sciencedirect.com
ScienceDirect
Ceramics International 33 (2007) 1341–1347
CERAMICS INTERNATIONAL
www.elsevier.com/locate/ceramint

Structure and crystallization kinetics of $PbO–B_2O_3$ glasses

Yin Cheng [a], Hanning Xiao [a,b,*], Wenming Guo [b], Weiming Guo [b]

[a] College of Materials Science and Engineering, Changsha University of Science & Technology, Changsha 410076, China
[b] College of Materials Science and Engineering, Hunan University, Changsha 410082, China

Received 17 January 2006; received in revised form 13 March 2006; accepted 15 April 2006
Available online 26 September 2006

Abstract

Structure and crystallization kinetics of $PbO–B_2O_3$ glasses containing 10–80 mol% PbO were investigated. The analyses of IR spectra reveal that PbO causes a change in the short-range order structure of the borate matrix. Between $10 \leq PbO \leq 20$ mol%, PbO only acts as a network modifier. With the increase of PbO content, a progressive conversion of $[BO_3]$ to $[BO_4]$ units occurs and this promotes the formation of boron–oxygen rings, composed of the connection of bridge oxygen between $[BO_3]$ and $[BO_4]$ units. When the content is over 60 mol%, PbO plays the role of glass former. Four possible structure models have been suggested to explain the effects of PbO on glass network: (a) three coordinated boroxol rings modified by Pb^{2+}; (b) formation of Pb–O–B covalent bands; (c) bridge networks between $[BO_3]$ and $[BO_4]$ units; (d) complex structures of Pb^{2+} modified boron–oxygen rings and chains. Moreover, The crystallization kinetics of $PbO–B_2O_3$ glasses was characterized by DSC analyses. When $PbO \geq 50$ mol%, the increase of PbO leads to a decrease of thermal stabilities of the glasses. The increase of B_2O_3 contributes to the increase trends to crystallization of glasses.

Keywords: C. Thermal properties; Lead borate glasses; Crystallization kinetics; Glass structure

1. Introduction

Lead borate glasses are of technological interests owing to their unique properties such as their low melting temperatures, wide glass formation regions and good radiation shielding properties, etc. [1–4]. During the past two decades, many efforts have been taken to help realize the roles of PbO in glass networks using different techniques [5–7]. Bray et al. [8] have carried out NMR investigations of lead borate glasses and their study indicates that N_4 (the fraction of the four coordinated boron atoms in the glass) increases with the PbO content up to 50 mol%, then decreases with the content of PbO. Raman spectroscopy investigations of $PbO–B_2O_3$ glasses [9] show that, above 50 mol% PbO, four coordinated boron ions convert into three coordinated boron ions. Not much IR spectroscopic work has been carried out in lead borate glasses with the exception of the preliminary work of Trate and Pottier [10], in which the low frequency IR peaks involving PbO vibrations were observed, indicating the appearance of new bands characteristic of covalent PbO bonds with the increased content of PbO. However, the role of PbO in different glasses does not understand clearly. The purpose of this work is to identify the network structure of $PbO–B_2O_3$ glasses and analyse the effects of PbO on modified borate glasses.

2. Theoretical basis

Differential scanning calorimetry (DSC) is very suitable for determinating the kinetic parameters of glass crystallization under non-isothermal conditions [11–13]. The modified Johnson–Mehl–Avrami (JMA) equation is well-known to describe the behaviour of non-isothermal glass crystallization [14]:

$$\ln[-\ln(1-\alpha)] = -n\ln b - 1.052\frac{mE_G}{RT} + \text{constant} \quad (1)$$

where α is the volume fraction of crystals precipitated in glass. It can be estimated by the area of crystallization exothermal peak [15], as shown in Fig. 1. α is the ratio of S_α/S. n and m are numerical factors depending on the nucleation process and growth morphology. When nuclei formed during the heating process at constant rate b are dominant, n is equal to $(m + 1)$ and when nuclei formed in the previous heat treatment before thermal analysis run are dominant, n is equal to m. The values of n and m are listed in Table 1 [12]. R is the universal gas

* Corresponding author. Tel.: +86 731 8822269; fax: +86 731 2617678.
E-mail address: hnxiao@hnu.cn (H. Xiao).

0272-8842/$32.00 © 2006 Published by Elsevier Ltd and Techna Group S.r.l.
doi:10.1016/j.ceramint.2006.04.025

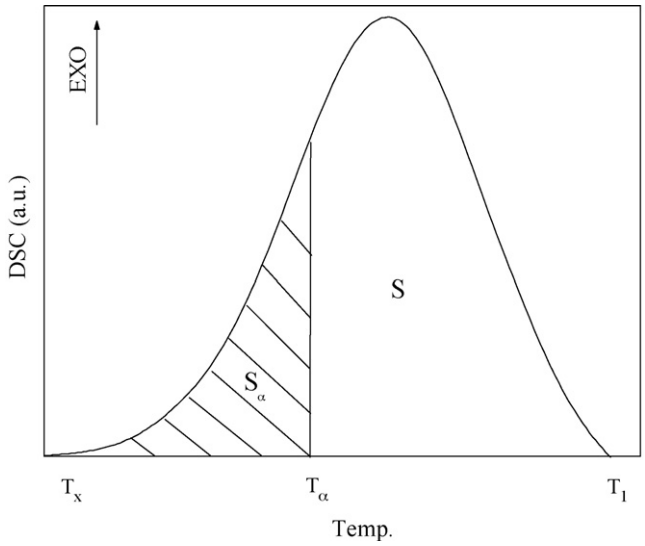

Fig. 1. Estimation of the volume fraction of crystals. T_x and T_l are the onset temperature and end temperature of exothermic peak, respectively; S is the total area of crystallization exothermal peak; S_α is partial area between T_x and T_l. α is the ratio of S_α/S.

constant. E_G is the activation energies for crystal growth. The effective activation energy of the crystallization process E can be defined by $E = (m/n)E_G$.

At the basis of Eq. (1), simple determination of E_G and n can be given by Šatava method [16]:

$$\left.\frac{\mathrm{d}\ln[-\ln(1-\alpha)]}{\mathrm{d}(1/T)}\right|_b = -1.052\frac{mE_G}{R} \tag{2}$$

and modified Ozawa–Chen method [17,18]:

$$\left.\frac{\mathrm{d}(\ln b)}{\mathrm{d}(1/T)}\right|_\alpha = -1.052\frac{m}{n}\frac{E_G}{R} \tag{3}$$

DSC is also helpful to determine the glass characteristic temperatures, such as glass transition temperature T_g, onset crystallization temperature T_x, and liquidus temperature T_l. These thermal parameters are suitable for a qualitative estimation of the thermal stability of glasses and the glass forming ability.

A parameter usually employed to estimate the glass stability is the thermal stability, which is defined by $\Delta T = T_x - T_g$ [19]. Another parameter introduced by Hruby [20,21] is the glass forming ability (k_{gl}) which is defined by the relation:

$$k_{gl} = \frac{T_x - T_g}{T_l - T_x} \tag{4}$$

Both an increasing difference $\Delta T = T_x - T_g$ or a decreasing temperature interval $T_l - T_x$ indicate an increasing glass stability and a lower tendency toward crystallization.

Table 1
The values of n and m for various crystallization mechanisms [12]

Mechanism	n	m
Bulk crystallization		
Three-dimensional growth	4	3
Two-dimensional growth	3	2
One-dimensional growth	2	1
Surface crystallization	1	1

3. Experiments

The PbO–B_2O_3 glasses, in the content of PbO from 10 to 80 mol%, were prepared by the conventional melting-quenching method with AR grade PbO and B_2O_3 as raw materials. After homogenization, the batches were melted in the temperature range of 700–1000 °C and the resulting liquid cooled in graphite mould, then crystallized at crystallization peak temperatures for 1 h. The compositions of glasses are shown in Table 2. When the content of PbO $\geq$ 30 mol%, transparent and homogeneous glasses were obtained. Bulk crystallization and surface crystallization were observed upon cooling in samples of PbO content equal to 10 and 20 mol%, respectively.

The infrared spectra of the glasses were recorded at room temperature, immediately after glass preparation, using KBr disc technique. A Rayleigh WQF-410 FTIR spectrometer was used to obtain the spectra in the wave number range between 400 and 2000 cm^{-1} with a resolution of 2 cm^{-1}. DSC measurements were performed by NETZSCH STA449C calorimeter at different heating rates (5, 10, and 20 °C min^{-1}). 1). SEM investigations were carried out with surface corrosion using JEOL JSM-5610LV electron microscope, operating in the secondary electron emission mode.

4. Results

The infrared absorption spectra of PbO–B_2O_3 glasses are shown in Fig. 2, including the IR spectra of pure B_2O_3 glasses. Tables 3 and 4 summarized the major observed absorption bands in the investigated glasses and their vibration types, respectively. It is clear from Fig. 2 and Table 3 that spectras of PB-1 and PB-2 samples are similar to that of pure B_2O_3 glasses, having two broad absorption bands at 1300–1700 and 720 cm^{-1}. Other glasses have three main absorption bands at 870–945, 680–702 and 1167–1360 cm^{-1}. When the content of PbO exceeds 60 mol%, several absorption bands below 600 cm^{-1} are also observed. Increasing the PbO content from 30 to 80 mol%, the 945 and 1360 cm^{-1} bands shift to lower frequency, while 681 cm^{-1} band changes to 702 cm^{-1}.

Table 2
The molar compositions of PbO–B_2O_3 glasses

No.	PB-1	PB-2	PB-3	PB-4	PB-5	PB-6	PB-7	PB-8
Compositions	$0.1PbO^{\bullet}$ $0.9B_2O_3$	$0.2PbO^{\bullet}$ $0.8B_2O_3$	$0.3PbO^{\bullet}$ $0.7B_2O_3$	$0.4PbO^{\bullet}$ $0.6B_2O_3$	$0.5PbO^{\bullet}$ $0.5B_2O_3$	$0.6PbO^{\bullet}$ $0.4B_2O_3$	$0.7PbO^{\bullet}$ $0.3B_2O_3$	$0.8PbO^{\bullet}$ $0.2B_2O_3$

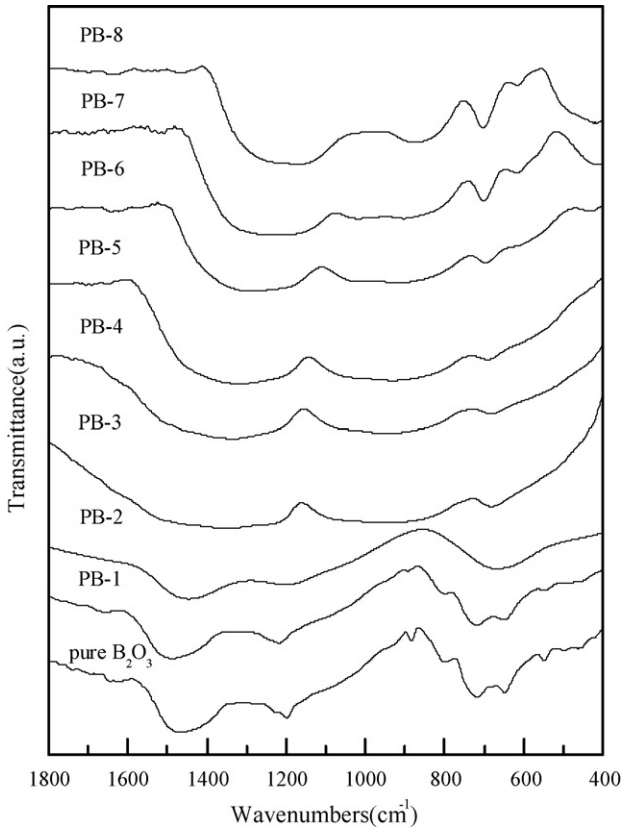

Fig. 2. Infrared absorption spectra of PbO–B_2O_3 glasses.

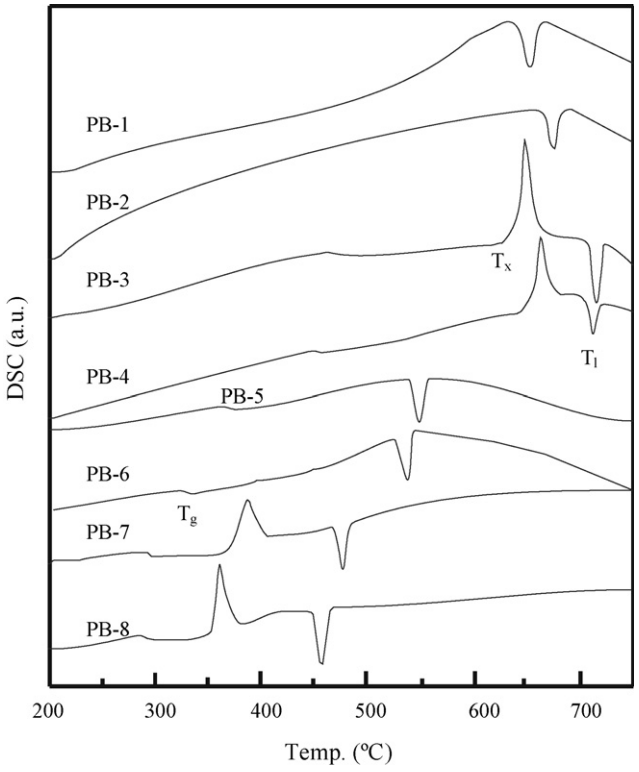

Fig. 3. DSC curves for PbO–B_2O_3 glasses.

Table 3
Observed IR absorption bands in PbO–B_2O_3 glass system (from Fig. 2)

No.	IR absorption bands (cm^{-1})							
B_2O_3 glass	1645	1460	1370			721		
PB-1	1641	1463	1356			717		
PB-2	1587	1452	1350			696		
PB-3			1361		945	681		
PB-4			1338		943	683		
PB-5			1315		931	690		
PB-6			1284	1016	916	696		424
PB-7			1234	1020	903	702	617	424
PB-8			1167		876	702	617	415

Table 4
Vibration types of different IR wave numbers

Range of wave numbers (cm^{-1})	Vibration types
≤620	Characteristic vibration of PbO [24]
680–720	Bending vibration of B–O–B in [BO_3] triangles [22,23]
900–950, 1000–1020	Stretching vibration of [BO_4] units [26]
About 1300	Vibration of boron–oxygen rings [29]
1300–1600	Stretching vibration of B–O–B in [BO_3] triangles [22,23]

The DSC curves from the different stoichiometries were indicated in Fig. 3. Values of characteristic temperatures summarized in Table 5 were extracted using the Proteus software installed in the DSC instrument. T_g was the inflection temperature of glass transition, T_x was the onset temperature of exothermic peak, and T_l was the peak point of endothermic peak for melting. When the content of PbO ≤ 30 mol%, both exothermic and endothermic peaks are not observed, which is due to the crystallization during cooling process. It is well-known that crystallized glasses, relatively stabilized, have no exothermal and endothermal changes during heating treatments. In the region of 50 ≤ PbO ≤ 60 mol%, there is no any exothermic peak observed, indicating that glasses in this composition region are stable on heating against crystallization; Therefore, calculations of crystallization kinetics are carried out only at the compositions of PB-3, PB-4, PB-7, PB-8 samples.

Table 5
Glass transition temperature T_g, onset crystallization temperature T_x, liquidus temperature T_l, and glass thermal stability parameters ΔT, k_{gl}

No.	T_g (°C)	T_x (°C)	T_l (°C)	ΔT (°C)	k_{gl}
PB-1			656.0		
PB-2			673.2		
PB-3	466.1	626.3	717.2	160.2	1.76
PB-4	449.6	647.5	703.6	197.9	3.53
PB-5	360.4		537.0		
PB-6	327.6		522.1		
PB-7	297.6	364.5	469.1	66.9	0.64
PB-8	291.8	355.3	499.7	63.5	0.44

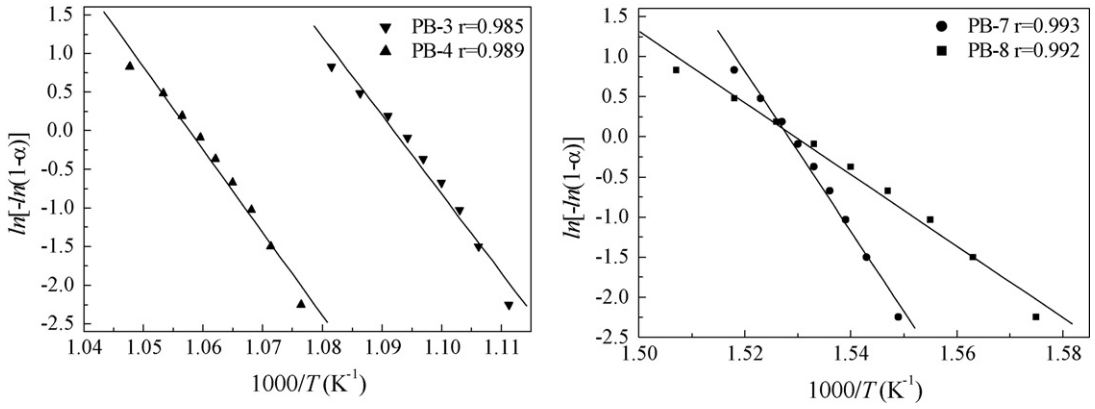

Fig. 4. Determination of mE_G according tothe Šatava method by plotting ln[−ln(1 − α)] vs.1/T at heating rate b = 10 °C min^{-1}. r is the correlative coefficient of linear fitting.

Šatava method (Eq. (2)) was used to evaluate the values of mE_G and a constant heating rates at 10 °C min^{-1} was assumed, as shown in Fig. 4. The volume fraction of crystals α of each sample in Fig. 4 was the same and lied in the range of 0.1–0.9. The correlation coefficients r of the plots are all greater than 0.99 indicating good linear relationships. The values of $E = (m/n)E_G$ were calculated by Ozawa–Chen method (Eq. (3)) at the range of α = 0.3–0.6, as shown in Fig. 5. The mean value at different values of α was chosen as the effective energy E for each sample, which was listed in Table 6. The values of n were evaluated by the ratio of mE_G/E, while m was the round number of $n - 1$ assuming that nucleation rate is constant ($n = m + 1$). E_G was estimated by combined the results above. Table 6 summarized all values of the kinetic parameters above.

SEM micrographs of crystallized samples are shown in Fig. 6. It is clear that different compositions lead to different types of crystals: PB-3 is spherical, PB-4 is lamellar, while PB-7 and PB-8 are columnar and needle-like, respectively.

5. Discussion

As seen from Fig. 2, the IR spectrums of the glasses containing 10–20 mol% PbO resemble that of pure B_2O_3. Two main absorption bands are included: a weak one at about

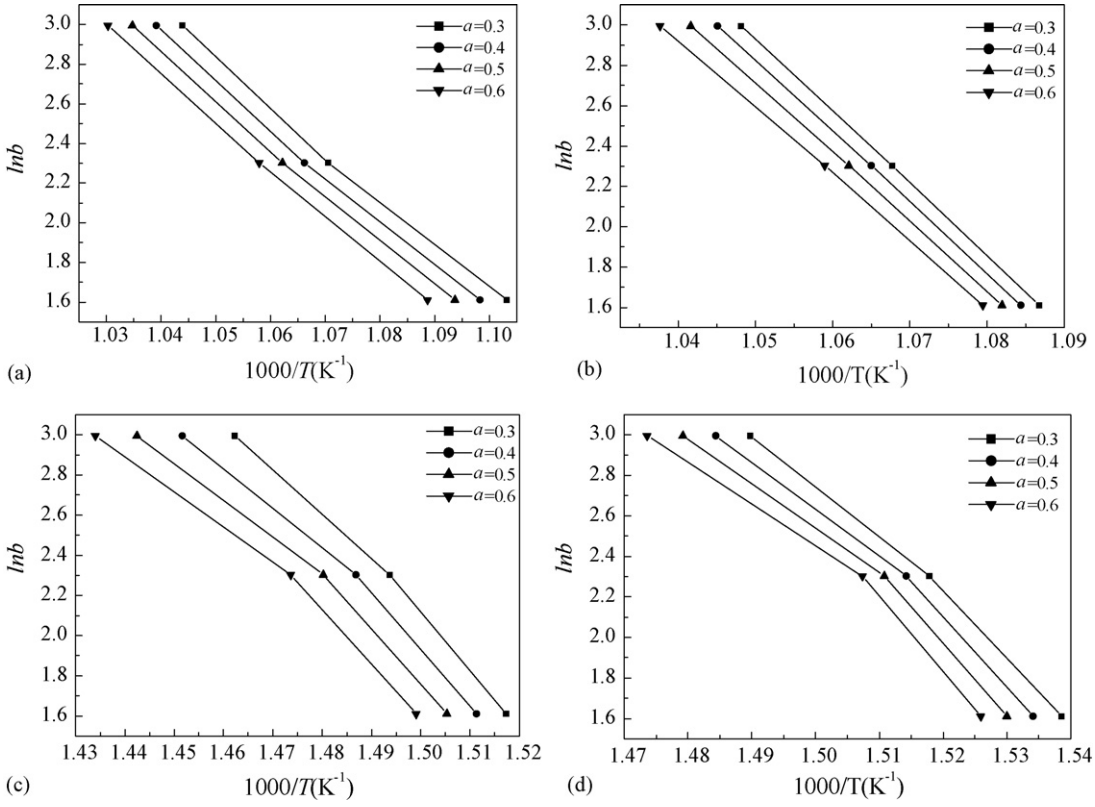

Fig. 5. Ozawa–Chen plot (ln b vs. 1/T_a) for determination of $E = (m/n)E_G$ at different values of a: (a) PB-3; (b) PB-4; (c) PB-7; (d) PB-8.

Table 6
Kinetic parameters of crystallization of the binary $PbO–B_2O_3$ glass system calculated by different methods

No.	n	m	mE_G (kJ/mol)	E_G (kJ/mol)	$E = (m/n)E_G$ (kJ/mol)
PB-3	3.89	3	809.16	269.72	208.01
PB-4	3.06	2	839.55	365.91	274.35
PB-7	3.68	3	787.55	262.52	213.98
PB-8	1.98	1	352.39	352.39	177.98

720 cm^{-1} and a broad one between 1300 and 1600 cm^{-1}. These two bands are attributed to the bending vibration and stretching vibration of B–O–B in $[BO_3]$ triangles [22,23], respectively. However, the band between 1300 and 1600 cm^{-1} of the modified glasses seem to be broader than that of pure B_2O_3. This suggests that the borate network is not modified by the addition of 10–20 mol% PbO, since only three-coordinated boron atoms can be identified. Further more, there is no evidence of absorption bands below 620 cm^{-1}, which are the characteristic vibration frequency of PbO [24]. Therefore, in this case PbO can be considered as a network participant filled in the interspaces of $[BO_3]$ units in the form of Pb^{2+} ion (see Fig. 7a).

When the content of PbO exceeds 30 mol%, an increasing trend (from 680 to 702 cm^{-1}) is observed in the bending vibration frequency of B–O–B in $[BO_3]$ units with the increasing PbO content. This behaviour may be attributed to the electrostatic field of the strongly polarizing Pb^{2+} ions, which might serve to increase the wave number of B–O–B bending vibration [25]. On the other hand, a new broad band between 900 and 950 cm^{-1} is observed, which is due to the stretching vibration of $[BO_4]$ units [26]. This indicates that the addition of PbO leads to the conversion of $[BO_3]$ units to $[BO_4]$ units in borate glass, which is also discovered in glass of $CeO_2–B_2O_3$, $La_2O_3–B_2O_3$ [27,28]. Moreover, with the increase of the content of PbO from 30 to 50 mol%, the frequency of $[BO_4]$ unit shifts from 945 cm^{-1} to a lower wave number 931 cm^{-1}. This may be due to the formation of bridging bond of Pb–O–B, as seen in Fig. 7b. Since the stretching force constant of Pb–O bonding is substantially lower than that of the B–O, the stretching frequency of Pb–O–B might trend to be lower.

Another dominant shift in the glass ($30 \leq PbO \leq 50$ mol%) is the sharp decreasing trend from 1360 to 1315 cm^{-1}. Boulos and Kreidl [29] attributes the broad bond of about 1300 cm^{-1} to the vibration of boron–oxygen rings composed by $[BO_3]$ and $[BO_4]$ units. Therefore, the presumption that boron–oxygen rings are formed in the glasses by the connection of the bridge oxygen ions between $[BO_3]$ triangles and $[BO_4]$ tetrahedrons can be made (see Fig. 7c), due to the decreasing frequency of the stretching vibration of B–O–B.

Subsequent additions of PbO (60–80 mol%) have the same effect on the structure of glasses. The biggest shift of 916–876 cm^{-1}, observed in PB-8 sample, indicates that when the content of PbO is up to 80 mol%, the content of Pb–O–B becomes dominant in the glass network structure. It can be presumed that the increasing polarization of Pb^{2+} with the increase content of PbO contributes to the formation of Pb^{2+} modified boron–oxygen rings and chains. New bands at 1016

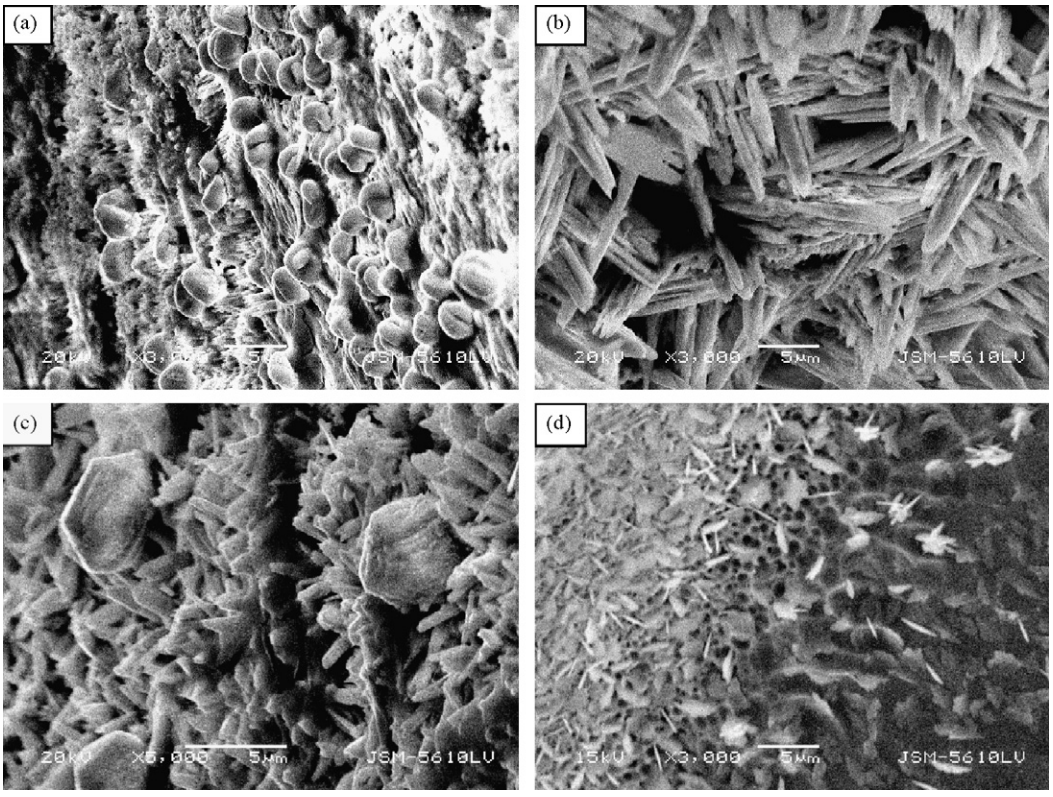

Fig. 6. SEM micrographs of crystallized samples (a) PB-3; (b) PB-4; (c) PB-7; (d) PB-8.

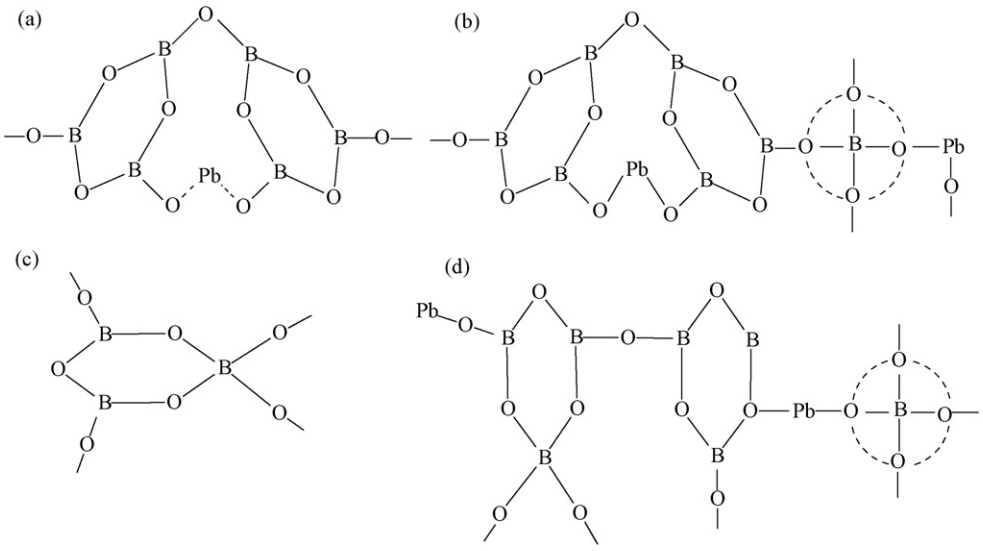

Fig. 7. Possible structural units of PbO–B_2O_3 glasses: (a) three coordinated boroxol rings modified by Pb^{2+}; (b) formation of Pb–O–B covalent bands; (c) bridge networks between [BO_3] and [BO_4] units; (d) complex structures of Pb^{2+} modified boron–oxygen rings and chains.

and 1020 cm^{-1} of PB-6 and PB-7 glasses can be attributed to the absorption vibration of [BO_4] units [26], indicating the increasing content of [BO_4] units in glass networks. The absorptions of PbO (below 620 cm^{-1}) show that PbO is one of the network former of glasses in this region. In light of the above discussions, it can be concluded that as PbO content exceeds 60 mol%, five bridging oxygens may be involved in glass networks: B–O–B in [BO_3] and [BO_4] units, the bridging oxygen ions between [BO_3] and [BO_4] units, Pb–O–B in bridge connection of [BO_3] and [BO_4] units, and Pb–O in covalent bonds, as seen in Fig. 7d.

From the obtained data of the kinetic criteria ΔT, k_{gl} (Table 5) and the activation energies (Table 6), it is possible to make some conclusions for the competitive role of PbO and B_2O_3 as a potential network former. It can be seen (Table 3) that an increase content of PbO leads to a decrease of T_g, and the change of glass thermal stabilities can be divided into four regions: (1) when PbO is below 20 mol%, surface crystallization and bulk crystallization are emerging, respectively, during cooling processes, indicating the most unstable glass compositions; (2) for $30 \leq PbO \leq 40$ mol%, first exothermal peaks of glasses appear at 600–650 °C, and increasing PbO content helps to decrease the trend to crystallization and improve stabilities of glasses, as seen from the increase of kinetic parameters and the activation energies E; (3) glasses in the composition region of $50 \leq PbO \leq 60$ mol%, are stabilized glasses against crystallization, since there are no exothermal peaks during heat treatments; (4) PbO $\geq$ 70 mol%, T_x appear at a relatively lower range of 350–360 °C and the values of E decrease, indicating that a further increase of PbO causes a decrease of thermal stabilities of the glasses.

The different values of n and m indicate the different crystallization mechanisms. Following the results in Tables 1 and 6, both PB-3 and PB-7 belong to the three-dimensional growth mechanisms, PB-4 corresponds to two-dimensional growth, the crystal growth of PB-8 glass is controlled by one-dimensional growth mechanism, which are consistent with the results of SEM observations (Fig. 6).

6. Conclusions

The content of PbO is responsible for the variation of the structure and crystallization kinetics of PbO–B_2O_3 ($10 \leq PbO \leq 80$ mol%) glasses. For $10 \leq PbO \leq 20$ mol%, the structure of glasses resemble that of pure B_2O_3, PbO only acts as a network modifier in the form of Pb^{2+}, and the glass compositional region is unstable; between $30 \leq PbO \leq 60$ mol%, the increase of PbO causes a progressive conversion of [BO_3] units to [BO_4] units, impairs the trend to crystallization and improves stability of glasses; with the further increase of PbO, the thermal stabilities of glasses decrease, and PbO plays the role of a glass former.

References

[1] Z. Pan, S.H. Morgan, B.H. Long, Raman scattering cross-section and non-linear optical response of lead borate glasses, J. Non-Cryst. Solids 185 (1995) 127–134.
[2] J.-M. Wu, H.-L. Huang, Microwave properties of zinc, barium and lead borosilicate glasses, J. Non-Cryst. Solids 260 (1999) 116–124.
[3] P. Srivastava, S.B. Rai, D.K. Rai, Effect of lead oxide on optical properties of Pr^{3+} doped some borate based glasses, J. Alloys Compd. 368 (2004) 1–7.
[4] N. Singh, K.J. Singh, K. Singh, H. Singh, Comparative study of lead borate and bismuth lead borate glass systems as gamma-radiation shielding materials, Nucl. Instr. Methods Phys. Res. B 225 (2004) 305–309.
[5] H.S. Liu, T.S. Chin, S.W. Yung, FTIR and XPS studies of low-melting PbO–ZnO–P_2O_5 glasses, Mater. Chem. Phys. 50 (1997) 1–10.
[6] D. Stentz, S. Blair, C. Goater, S. Feller, M. Affatigato, Analysis of the structure of lead borosilicate glasses using laser ionization time of flight mass spectroscopy, J. Non-Cryst. Solids 293/295 (2001) 416–421.
[7] M. Abid, M. Et-Tabirou, M. Taibi, Structure and DC conductivity of lead sodium ultraphosphate glasses, Mater. Sci. Eng. B 97 (2003) 20–24.

[8] P.J. Bray, M. Leventhal, H.O. Hooper, Nuclear magnetic resonance investigations of the structure of lead borate glasses, Phys. Chem. Glasses 4 (1963) 47–66.
[9] B.N. Meera, A.K. Sood, N. Chandrabhas, J. Ramakrishna, Raman study of lead borate glasses, J. Non-Cryst. Solids 126 (1990) 224–230.
[10] P. Tarte, M.J. Pottier, in: P.H. Gaskell (Ed.), The Structure of Non-Crystalline Solids, 1976, p. 227.
[11] C. Dayanand, M. Salagram, Thermal (DSC) characterization of xPbO–$(1-x)P_2O_5$ glass system, Ceram. Int. 30 (2004) 1731–1735.
[12] R. Iordanova, E. Lefterova, I. Uzunov, D. Klissurshi, Non-isothermal crystallization kinetics of V_2O_5–MoO_3–Bi_2O_3 glasses, J. Therm. Anal. Cal. 70 (2002) 393–404.
[13] K. Yukimitu, R.C. Oliveira, E.B. Araújo, J.C.S. Moraes, L.H. Avanci, DSC studies on crystallization mechanisms of tellurite glasses, Thermochim. Acta 426 (2005) 157–161.
[14] H. Yinnon, D.R. Uhlmann, Applications of thermoanalytical techniques to the study of crystallization kinetics in glass-forming liquids, part I: theory, J. Non-Cryst. Solids 54 (1983) 253–275.
[15] C.S. Ray, W.H. Huang, D.E. Day, Crystallization kinetics of a lithia-silica glass: effect of sample characteristics and thermal analysis measurement techniques, J. Am. Ceram. Soc. 74 (1991) 60–66.
[16] V. Šatava, Mechanism and kinetics from non-isothermal TG traces, Thermochim. Acta 2 (1971) 423–428.
[17] H.S. Chen, A method for evaluating viscosities of metallic glasses from the rates of thermal transformations, J. Non-Cryst. Solids 27 (1978) 257–263.
[18] T. Ozawa, Bull. Chem. Soc. Jpn. 38 (1965) 1881.
[19] S. Mahadevan, A. Giridhar, A.K. Singh, Calorimetric measurements on As–Sb–Se glasses, J. Non-Cryst. Solids 88 (1986) 11–34.
[20] A. Hruby, Evaluation of glass-forming tendency by means of DTA, Phys. B 22 (1972) 1187–1193.
[21] A. Hruby, Glass-forming tendency in the GeSx system, Phys. B 23 (1973) 1263–1272.
[22] E.I. Kamitsos, A.P. Patsis, M.A. Karakassides, G.D. Chryssikos, Infrared reflectance spectra of lithium borate glasses, J. Non-Cryst. Solids 126 (1990) 52–67.
[23] A.K. Hassan, L. BÖrjesson, L.M. Torell, The boson peak in glass formers of in creasing fragility, J. Non-Cryst. Solids 172/174 (1994) 154–160.
[24] W.L. Konijnendijk, H. Verweij, Structural aspects of vitrous PbO–$2B_2O_3$ studied by Raman scattering, J. Am. Ceram. Soc. 59 (1976) 459–461.
[25] K. El-Egili, H. Doweidar, Y.M. Moustafa, I. Abbas, Structure and some physical properties of PbO–P_2O_5 glasses, Phys. B 339 (2003) 237–245.
[26] G. El-Damrawi, K. El-Egili, Characterization of novel CeO_2–B_2O_3 glasses, structure and properties, Phys. B 299 (2001) 180–186.
[27] P.J. Bray, B^{10} NMR studies of the structure of borate glasses, J. Non-Cryst. Solids 38/39 (1980) 93–98.
[28] J. Lorosch, M. Couzi, J. Pelous, R. Vacher, A. Levasseur, Brillouin and Raman scattering study of borate, J. Non-Cryst. Solids 69 (1984) 1–25.
[29] E.N. Boulos, N.J. Kreidl, Structure and properties of silver borate glasses, J. Am. Ceram. Soc. 54 (1971) 368–373.